

## Feasibility of flow studies at NICA/MPD

N. S. Geraksiev<sup>1,2\*</sup> for the MPD collaboration

<sup>1</sup> Paisii Hilendarski University of Plovdiv, 24 Tsar Asen Str., BG-4000 Plovdiv, Bulgaria

<sup>2</sup> Veksler and Baldin Laboratory of High Energy Physics, Joint Institute for Nuclear Research, 141980 Dubna, Moscow region, Russia

In the light of recent developments in heavy ion physics, anisotropic flow measurements play a key role in a better understanding of the hot and dense baryonic matter. In the presented article a short introduction to the proposed NICA/MPD project is given, as well as a brief description of the event plane method used to estimate the elliptic flow of reconstructed and identified hadrons ( $p$ ,  $\pi$ ,  $K$ ,  $\Lambda$ ).

**Key words:** HEP, NICA, MPD, UrQMD, event plane, elliptic flow, hadron, hyperon

### INTRODUCTION

#### *Nuclotron-based Ion Collider fAcility (NICA)*

Investigation of the hot and dense baryonic matter is currently an exciting field in modern high energy physics. Besides being crucial to a better understanding of the early stages of the Universe and the formation of neutron stars, it is useful for the comprehension of in-medium properties of hadrons and nuclear matter equation of state, and may prove to be a means of search for manifestations of deconfinement and/or chiral symmetry restoration.

The Nuclotron upgrade, which is a substantial part of the JINR scientific program, is dedicated to the investigation of hot and dense baryonic matter.

The Nuclotron-based Ion Collider fAcility (NICA) will create Au+Au collisions over a wide range of atomic masses, at a centre-of-mass energy of  $\sqrt{s_{NN}} = 11A$  GeV (for  $Au^{79+}$ ) and an average luminosity of  $L = 10^{27} \text{cm}^{-2} \text{s}^{-1}$ , proton-proton collisions with  $\sqrt{s_{pp}} = 26A$  GeV and  $L = 10^{30} \text{cm}^{-2} \text{s}^{-1}$ .

Along with the heavy ion programme, the NICA facility will provide proton and light ion beams, and the possibility to obtain and utilize unique polarized beams. This holds a great potential for studies of the nuclear quark-gluon structure in processes with large momentum transfer, as well as in measurements with target/projectile polarization, and research on experimental verification of quark counting rules, clarification of the abnormal behavior known as color nuclear transparency, as well as comprehension of large spin effects in production of mesons and hyperons.

The accelerator will also allow collisions of mass-

\* To whom all correspondence should be sent:  
nikolay.geraksiev@gmail.com

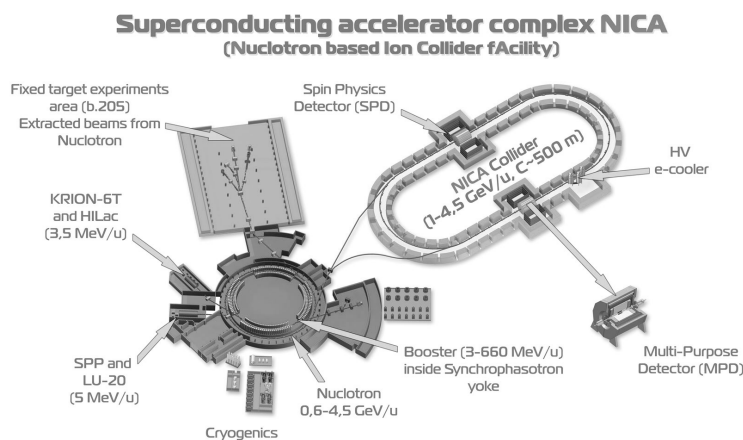


Fig. 1. The NICA accelerator complex at JINR

asymmetric beams including  $pA$  collisions. In and of itself an interesting field, it is also quite important as a reference point for comparison with heavy ion data. Furthermore, as a long-term goal, the accelerator facility may provide electron-ion collisions for measurements of nucleon and nuclei electro-magnetic form factors to large momenta, *e.g.* investigation of spatial distributions of charge and magnetization in nuclei and the nucleon including the determination of the valence quark generalized parton distribution, revealing the correlation between spatial and momentum distributions.

It should be noted that while the NICA project is aimed at fundamental scientific research, other applications of the particle beams such as biomedical research and radiation technology have been planned [1, 2].

### MultiPurpose Detector (MPD)

The NICA collider is going to have two interaction points, allowing for two detectors to operate simultaneously. The MultiPurpose Detector (MPD) is one of these detectors. In the first stage of the NICA/MPD project are considered analyses on multiplicity and spectral characteristics of identified hadrons including strange particles, multi-strange baryons and antibaryons, characterizing entropy production and system temperature at freeze-out. Moreover, event-by-event fluctuations in multiplicity, charges, transverse momenta and  $K/\pi$  ratios are to be studied as a generic property of critical phenomena, along with collective flow effects, HBT correlation, and femtoscopy. In the second stage measurements of the electromagnetic probes (photons and dileptons) will be carried out. The MPD detector will be operated at a rate of about  $7 \times 10^3$  interactions per second, with multiplicities of up to  $\sim 1500$  charged particles per central gold-gold collision at maximal energy of  $\sqrt{s_{NN}} = 11A$  GeV [1–3].

The design of the detector requires a very low material budget as the average transverse momentum of the particles produced in a collision at NICA energies is below 500 MeV/c.

The barrel part, consisting of a tracker and particle identification system is shown in Fig. 2. The time projection chamber (TPC) is the principal tracker yielding precise track finding, momentum determination, vertex reconstruction and pattern recognition up to  $|\eta| < 2$ . The energy loss ( $dE/dx$ ) measurements

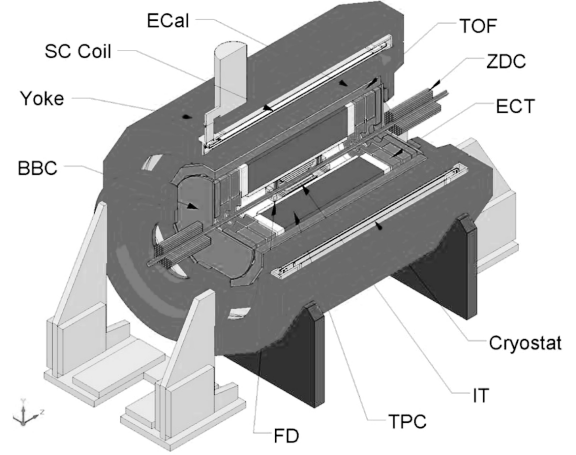


Fig. 2. Central part of the MultiPurpose Detector.

in the TPC gas will provide an additional capability for particle identification in the low momentum region [4].

The high performance time-of-flight (TOF) system must be able to identify charged hadrons and nuclear clusters in the broad rapidity range and up to total momentum of 2 GeV/c. The TOF detector covers  $|\eta| < 3$  and its performance should allow the separation of kaons from protons up to a total momentum of 3 GeV/c [5].

Fast timing and triggering is performed by arrays of quartz counters (FD). The forward going energy for centrality selection and event plane reconstruction will be measured by two sets of hadron calorimeters (ZDC), covering the pseudorapidity region  $2.5 < |\eta| < 4$  [6].

The main aim of the electromagnetic calorimeter (EMC) is identification of electrons and photons, and high precision measurements of their energy. The high granularity, excellent energy resolution and good timing performances of the EMC will enhance the overall efficiency and particle identification capabilities of the MPD detector [3, 7].

### ANISOTROPIC FLOW

Measurements of collective flow phenomena are crucial tools for the study of properties in the dense matter created in relativistic heavy ion collisions (such as the equation of state - EOS, formation conditions, *etc.*). The physics dynamics at the early stages of non-central heavy ion collisions is assessed by the azimuthal anisotropy of particle production with respect to the reaction plane [8].

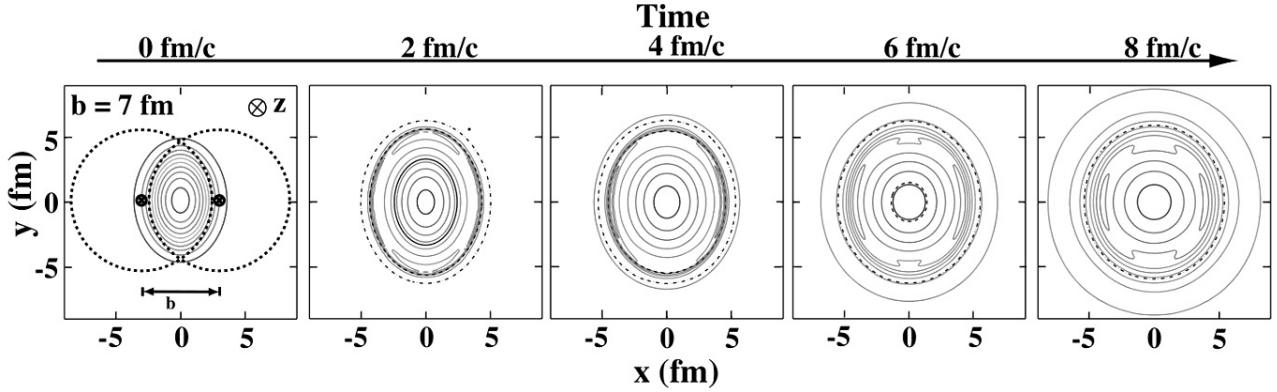


Fig. 3. Evolution of the transverse energy density profile in coordinate space for non-central heavy ion collisions.

The reaction plane is defined by the impact parameter and the beam direction  $z$ . The Fourier expansion of the invariant triple differential distributions proves to be a convenient way of characterizing the various patterns of anisotropic flow

$$E \frac{d^3N}{d^3\mathbf{p}} = \frac{dN}{p_T dp_T d\phi dy} \quad (1)$$

$$= \frac{1}{2\pi} \frac{dN}{p_T dp_T dy} \left( 1 + 2 \sum_{n=1}^{\infty} v_n \cos(n(\phi - \Psi_{RP})) \right),$$

where  $E$  is the energy of the particle,  $\mathbf{p}$  the momentum,  $p_T$  the transverse momentum,  $\phi$  the azimuthal angle,  $y$  the rapidity, and  $\Psi_{RP}$  the reaction plane angle. The sine terms in such an expansion vanish because of the reflection symmetry with respect to the reaction plane. The Fourier coefficients are  $p_T$  and  $y$  dependent and are given by

$$v_n(p_T, y) = \langle \cos(n(\phi - \Psi_{RP})) \rangle, \quad (2)$$

where the angular brackets denote an average over the particles summed over all events in the  $(p_T, y)$  bin under study. Fig. 3 depicts the evolution of the almond shaped interaction volume. Plots from left to right show how the system evolves from an almond shaped transverse overlap region into an almost symmetric system and contours indicate the energy density profile. During this expansion, governed by the velocity of sound, the created hot and dense system cools down [8].

The coefficient  $v_1$  is also known as directed flow and it presents a means of measuring the total amount of transverse flow. It is most pronounced in the cases of semi-central interactions around target and projectile rapidities where the spectators are deflected away

from the beam axis due to a bounce-off from the compressed and heated matter in the overlap region.

The elliptic flow is paid special attention as this collective motion is formed mainly at an early stage of the collision. According to the typical hydrodynamic scenario, the  $v_2(p_T)$  values at relatively low transverse momenta ( $p_T \lesssim 2$  GeV/c) are determined mainly by the internal pressure gradients of the expanding fireball during the initial high density phase of the reaction. The elliptic flow of hadrons at low transverse momenta can be related to the degree of thermalization, viscosity, and EoS of the produced matter. However, the elliptic flow of the high momentum particles is related to the jet fragmentation and energy loss of the primordially produced hard antiquark-quark pair traveling through the hot QCD medium. At moderate  $p_T$  the experimental data indicate a gradual increase of  $v_2$  with  $p_T$ . A deeper insight into the bulk properties of the produced matter is obtained by an accurate  $v_2$  measurement.

Two main reasons justify the increased demand for an accurate study of (anti)hyperon production. Firstly, a signature for deconfinement might be manifested by strangeness enhancement in heavy-ion collisions relative to proton induced reaction [9–11]. Secondly, due to the small hadronic cross-sections of multi-strange hyperons, additional rescattering effects in the dense hadronic matter for strange hadrons are not as significant as compared to other hadrons. Therefore, measurements of phase-space distributions of strange hyperons reveal key characteristics of the fireball at the early stages of the system evolution. Moreover, it has recently been observed by the STAR experiment that the characteristic azimuthal anisotropy pattern (*e.g.* the elliptic flow coefficient  $v_2$

as a function of transverse momentum  $p_T$ ) for anti-baryons is different from the one for baryons in mid-central Au+Au collisions at energies  $\sqrt{s_{NN}} < 11A$  GeV [12]. There is interplay between particle production and subsequent absorption in the medium meaning that anti-baryons are strongly affected by the co-moving baryon density in the course of the reaction. Different values of the collision energy and beam atomic mass number at NICA will provide a valuable insight into the reaction dynamics on (anti)hyperon production.

### ANALYSIS AND RESULTS

The analysis procedure was carried out using the MPDroot software (based on FairRoot) and the flow analysis package used by the STAR and ALICE experiments. Events were generated with the UrQMD 3.3 model, commonly used in heavy ion research [13, 14]. A total of  $3 \cdot 10^5$  gold-gold ( $\text{Au}^{79+}$ ) collisions with impact parameter in the range of 0–9 fm and energy  $\sqrt{s_{NN}} = 11A$  GeV were analyzed. The produced particles were transported through the TPC and TOF detectors using the GEANT3 transport package [15]. Tracks were reconstructed with the Kalman filtering technique [16]. In order to achieve a good precision of momentum and energy loss measurements, a track selection criteria of minimum 10 TPC points was required. The full range of TPC pseudorapidity was used ( $|\eta| < 2$ ). The reconstructed TPC tracks were extrapolated to the TOF detector and matched to TOF hits.

Table 1. Particle identification efficiency and contamination

| Particle                                      | $p, \bar{p}$ | $\pi^\pm$ | $K^\pm$ |
|---|--------------|-----------|---------|
| <b><math>P_{\text{trust}} &gt; 0</math></b>   |              |           |         |
| Efficiency, %                                 | 90.84        | 91.48     | 66.01   |
| Contamination, %                              | 22.92        | 7.25      | 43.76   |
| <b><math>P_{\text{trust}} &gt; 0.6</math></b> |              |           |         |
| Efficiency, %                                 | 82.41        | 83.62     | 47.41   |
| Contamination, %                              | 19.48        | 5.82      | 26.70   |

Several particle identification methods are available for the MPD experiment. For this particular study the Bayesian approach based on energy loss  $dE/dx$  from TPC and TOF  $M^2$  information was used (see [17]) to differentiate between track candidates' probabilities to be of certain particle species. For the elliptic flow study identification of charged hadrons ( $p, \pi, K$ ) was done in terms of highest probability *e.g.* if the track has the highest probability value to be that of a proton than say pion, we regard the track as to be that of a proton. A selection criteria threshold was introduced so that only tracks above a certain probability  $P_{\text{trust}}$  may be tagged. Particle identification quality was estimated (see Fig. 4 and Table 1) by efficiency and contamination as functions of transverse momentum

$$E^i = \frac{N_{\text{corr}}^i}{N_{\text{ana}}^i}, C^i = \frac{N_{\text{incorr}}^i}{N_{\text{Ncorr}}^i + N_{\text{incorr}}^i} \quad (3)$$

where  $E^i$  and  $C^i$  are the efficiency and contamination of a particle species  $i$ ,  $N_{\text{corr}}^i$  is the number of correctly

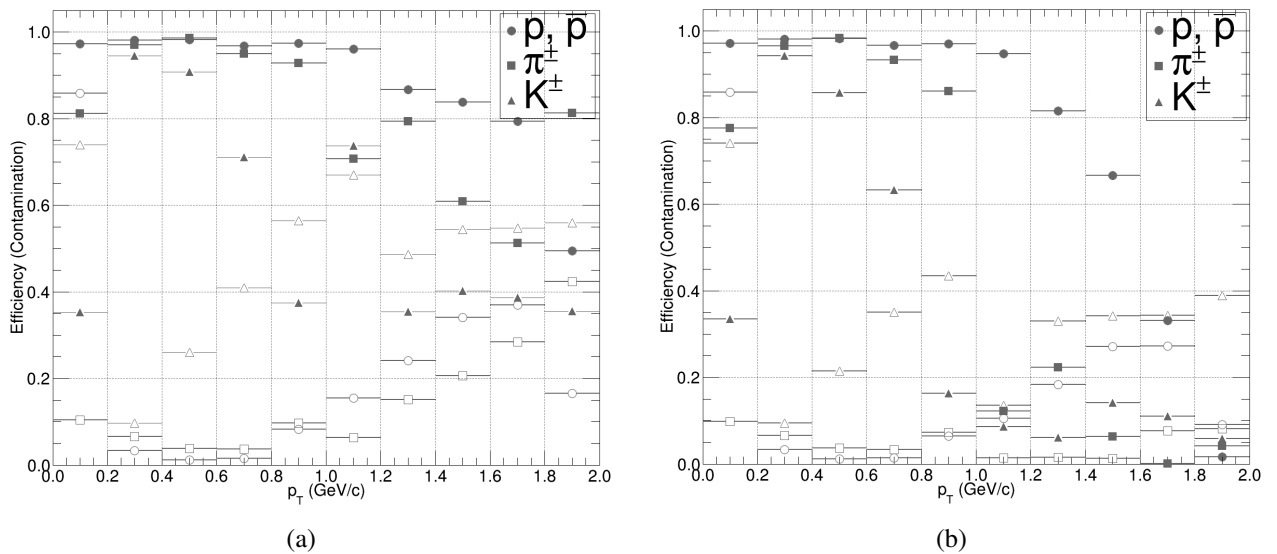


Fig. 4. Particle identification efficiency and contamination as a function of transverse momentum for probability thresholds of (a)  $P_{\text{trust}} > 0$  and (b)  $P_{\text{trust}} > 0.6$

where  $E^i$  and  $C^i$  are the efficiency and contamination of a particle species  $i$ ,  $N_{corr}^i$  is the number of correctly identified particles,  $N_{ana}^i$  - the number of generated particles with more than 10 points in TPC and  $N_{incorr}^i$  is the number of incorrectly identified particles.

It should be noted that particle identification plays a key role in elliptic flow determination and while the purpose of this study was not particle identification itself, the optimization of the identification criteria is to be carried out in subsequent studies.

### Event plane angle

A well established method of analysing the anisotropic flow is given in [18, 19]. The event plane angle was reconstructed by all identified charged tracks ( $P_{trust} \geq 0$ ) using two sub-events in negative and positive rapidity. The tracks in these sub-selections build sub-Q vectors from which two sub-event plane angles are then determined:

$$Q_{n,x} = \sum w_i \cos(n\phi_i) \quad (4)$$

$$Q_{n,y} = \sum w_i \sin(n\phi_i) \quad (5)$$

$$\Psi_n = \frac{1}{n} \arctan \left( \frac{Q_{n,y}}{Q_{n,x}} \right) \quad (6)$$

where the sum is carried on every selected track  $i$  in the sub-event,  $Q_{n,x}$  and  $Q_{n,y}$  are the components of the two-dimensional  $Q$ -vector,  $w_i$  are weight corrections,  $n$  denotes the order of Fourier harmonic expansion,  $\phi$  is the track azimuth angle and  $\Psi$  is the reconstructed event plane angle.

Event plane determination is sensitive to a non-uniform acceptance in azimuth angle, so weights are

used in  $\phi$ , additionally  $p_T$  weights are used to improve the event plane resolution. Other methods to correct for acceptance issues include recentering of the event or event mixing (both not used in this study). It should be noted that the UrQMD model has an event plane angle equal to a constant of zero. For convenience the event plane angle is shifted to positive values *e.g.*  $\Psi_1 \in [-\pi; +\pi] \rightarrow \Psi_1 \in [0; 2\pi]$  for the first harmonic ( $\Psi_2 \in [-\pi/2; +\pi/2] \rightarrow \Psi_2 \in [0; +\pi]$  for the second harmonic), which transforms the UrQMD event plane angle of 0 rad into  $\pi$  rad.

The results were fit with a Breit-Wigner function as a means of assessing event plane angle estimation versus centrality (impact parameter in this case), as shown in Fig. 5. The event plane resolution over all events is determined by:

$$R_n = \sqrt{2 \langle \cos(\Psi_{n,A} - \Psi_{n,B}) \rangle} \quad (7)$$

where  $R_n$  is the resolution for the  $n$ -th harmonic and  $\Psi_{A,B}$  are the sub-event plane angles. For this data set the resolution was calculated to be  $R_2 = 0.4805 \pm 0.0023$ . Alternatively, the approach of event-by-event resolution may be used for future studies [20]. One may argue that using the event plane resolution from two sub-events as a function of centrality may provide a more obvious illustration of EP determination quality than the provided Breit-Wigner fits, but that will be an objective for subsequent studies at higher statistics and a wider range of centrality selections. Furthermore, the Zero Degree Calorimeter may provide a complementary role in the event plane determination [6] which is also to be addressed in the future.

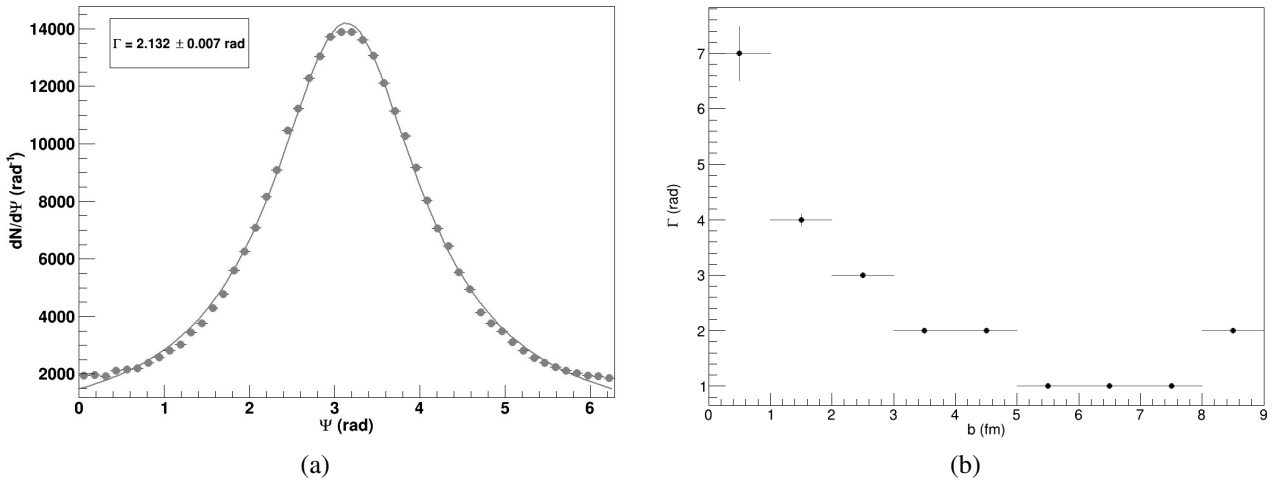


Fig. 5. (a) – reconstructed event plane angle  $\Psi_1$ , (b) – width of Breit-Wigner fit  $\Gamma$  versus the impact parameter  $b$

Elliptic flow of identified hadrons

Following the determination of the event plane angle and the corresponding resolution, particles are correlated to the event plane to reveal the observed differential distributions  $v_2^{obs}(p_T)$  and  $v_2^{obs}(y)$ , however they need to be corrected by the event plane resolution to obtain the final results given by  $v_2 = v_2^{obs}/R_2$ . The integrated elliptic flow coefficient was determined to be  $v_2 = 0.0266 \pm 0.0002$  which is in line with measurements made for the elliptic flow versus energy excitation function in several experiments (e.g. [21–23]). It should be noted that the integrated elliptic flow coefficient versus centrality and/or beam energy will also be goals for future studies.

In Fig. 6 are shown differential distributions of  $v_2(p_T)$  for probability trust thresholds. Misidentification of particles in the higher  $p_T$  region is more pronounced, so after applying the  $P_{trust} > 0.6$ , a more “pure” sample was derived at the cost of statistics, leading to a requirement of a larger data set and further investigation.

Elliptic flow of  $\Lambda$ -hyperons

Reconstruction of  $\Lambda(\bar{\Lambda})$ -hyperons was performed using the decay mode  $\Lambda \rightarrow p + \pi^-$ . The secondary vertex reconstruction utilizes a similar approach to the Kalman filtering formalism described in [24]. For the  $\Lambda$ -hyperon reconstruction the trust probability threshold was not used and tracks were tagged by means of highest probability.

The applied topological cuts are: distance of the closest approach (DCA) of the daughter particles to the primary vertex, small distance of separation in the decay vertex between the tracks, and relatively large decay length of the mother particle. Both the DCA and the two-track separation cuts should have increased efficiency if applied in  $\chi^2$ -space, i.e. when normalized to their respective errors.

The exact values of selection cuts were found by multidimensional scan over the whole set of selection criteria with a requirement to maximize the invariant mass peak significance. It is defined as  $S/\sqrt{S+B}$ , where  $S$  and  $B$  are total numbers of signal (described by

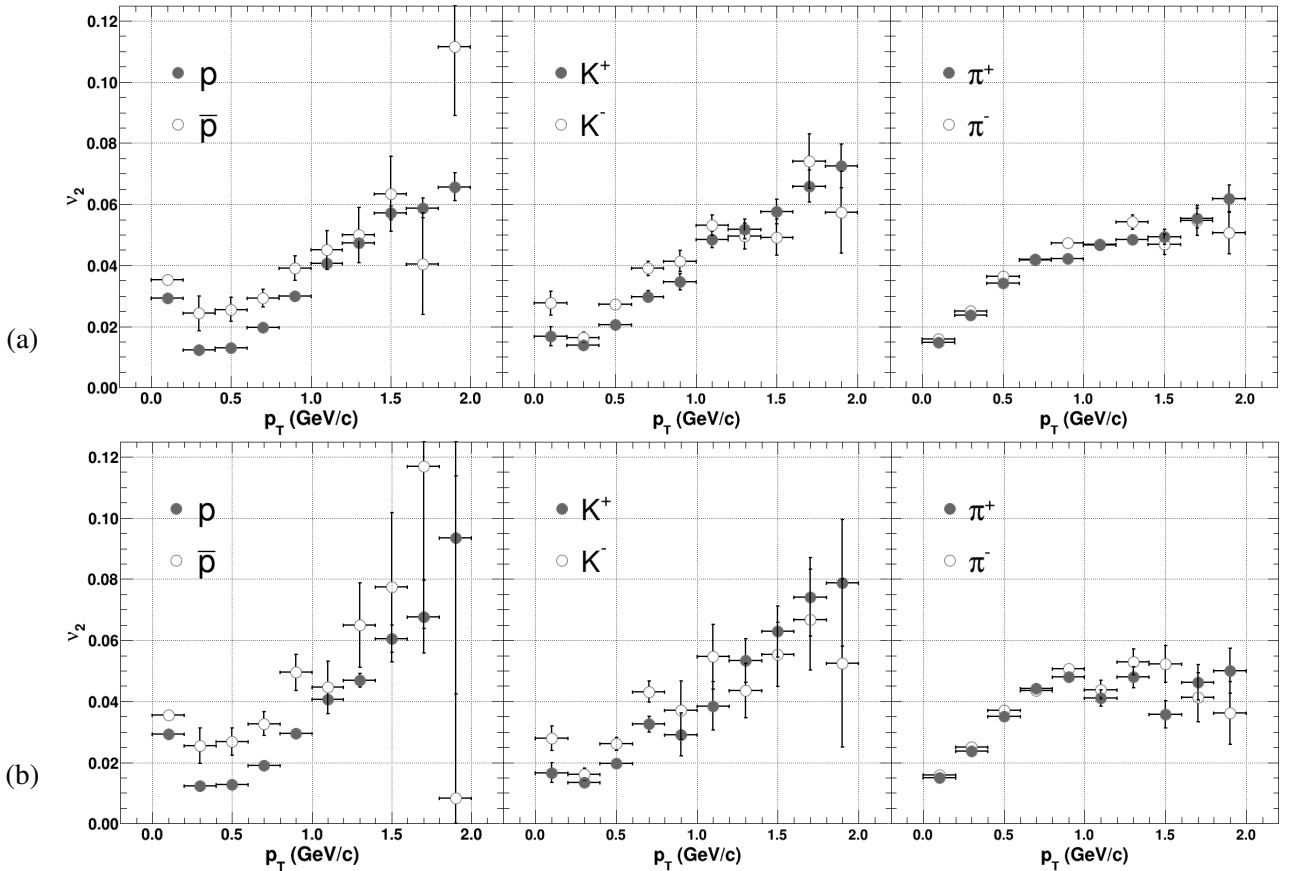


Fig. 6. Differential elliptic flow values in bins of transverse momentum, (a) –  $P_{trust} > 0$ , (b) –  $P_{trust} > 0.6$ .

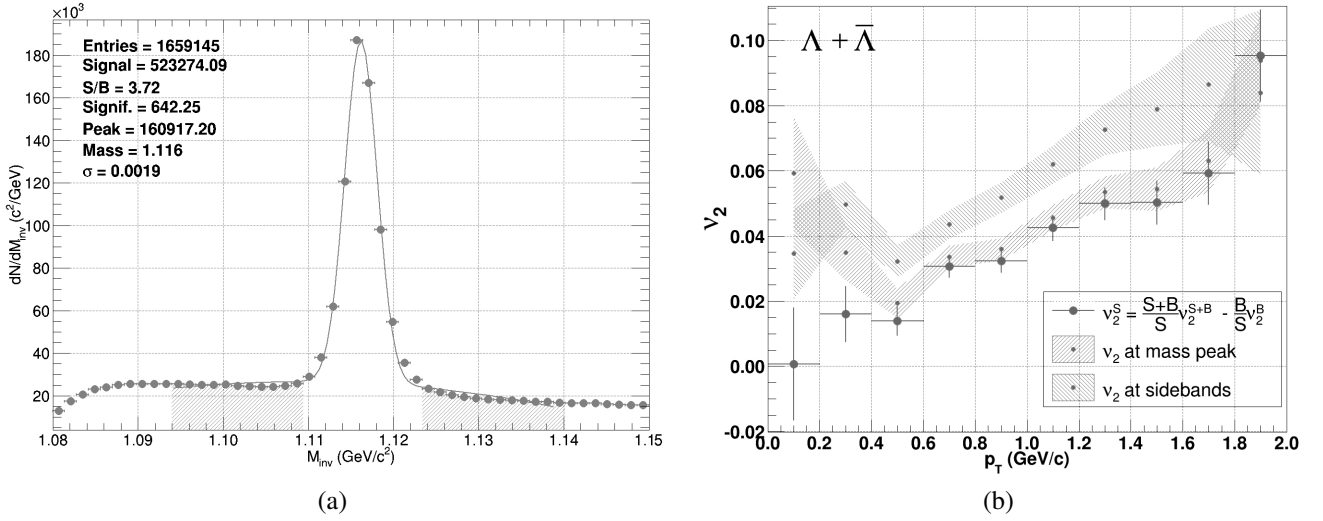


Fig. 7. (a) – Invariant mass distribution in bins of  $1.4 \text{ MeV}/c^2$  each, (b) –  $\Lambda, \bar{\Lambda}$ -hyperon elliptic flow

the gaussian) and background (polynomial function) combinations inside  $\pm 2\sigma$  interval around the peak position.

The selection cuts used for this study were optimized for  $\sqrt{s_{NN}} = 9A \text{ GeV}$  and it should be noted that better signal to background ratio may be achieved for the  $\sqrt{s_{NN}} = 11A \text{ GeV}$  data set used in this study. Moreover, for the flow analysis procedure the signal and background are evaluated in bins of  $p_T$  and optimal results can be obtained with further signal to background ratio maximization carried out in these bins.

The  $\Lambda$  elliptic flow is evaluated in the invariant mass peak region and in the sidebands region, and the background contribution is removed from the signal by

$$v_2^S = \frac{S+B}{S}v_2^{S+B} - \frac{B}{S}v_2^B \quad (8)$$

where  $v_2^S$  is the  $\Lambda$ -hyperon flow “pure” signal,  $v_2^{S+B}$  is the flow signal as measured in the mass peak region and  $v_2^B$  is the flow signal contribution by the background, measured in the hatched area (see Fig. 7 (a)). This approach of background subtraction is very straight forward and simple to implement, however, different methods of background subtraction may be added for comparison in further studies. In Fig. 7 (b) with markers is shown the  $v_2(p_T)$  differential flow calculated by (8) and the right and left hatched areas represent the measured flow in the mass peak and sideband regions respectively.

## CONCLUSIONS

A short description of the proposed NICA/MPD project was given. Several points have been made on the prospects of hadron flow studies and the important role hyperons may provide for the better understanding of the initial fireball conditions. Future improvements of the presented results of reconstructed and identified hadrons ( $p, \pi, K, \Lambda$ ) elliptic flow as well as an outlook on subsequent studies in this area of research have been noted.

## REFERENCES

- [1] NICA Conceptual Design Report, 2008, [http://nica.jinr.ru/files/NICA\\_CDR.pdf](http://nica.jinr.ru/files/NICA_CDR.pdf).
- [2] NICA White Paper, 2011, <http://nica.jinr.ru/files/WhitePaper.pdf>.
- [3] MPD Conceptual Design Report, 2011, [http://nica.jinr.ru/files/MPD\\_CDR\\_en.pdf](http://nica.jinr.ru/files/MPD_CDR_en.pdf).
- [4] MPD TPC Technical Design Report, 2013, [http://nica.jinr.ru/files/MPD/TPC\%20TDR-v1\\_2\\_1.pdf](http://nica.jinr.ru/files/MPD/TPC\%20TDR-v1_2_1.pdf).
- [5] V.Babkin, V.Golovatyuk, Yu.Fedotov, S.Lobastov, S.Volgin, N.Vladimirova, 2009, <http://nica.jinr.ru/files/TOF-MPD.pdf>.
- [6] M. B. Golubeva, F. F. Guber, A. P. Ivashkin, A. Yu. Isupov, A. B. Kurepin, A. G. Litvinenko, E. I. Litvinenko, I. I. Migulina, V. F. Peresedov, *Physics of Atomic Nuclei*, **76**, 1-15 (2013).
- [7] V. Kolesnikov and A. Zinchenko for the MPD Collaboration, preprint arXiv:1312.1091v1 [nucl-ex] (2013).

- [8] R. Snellings, preprint arXiv:1102.3010v2 [nucl-ex] (2011).
- [9] J. Rafelski and B. Muller, *Phys. Rev. Lett.* **48**, 1066 (1982).
- [10] F. Antinori et al. (WA97 Collaboration), *Eur. Phys. J. C* **11**, 79 (1999).
- [11] F. Antinori et al. (NA57 Collaboration), *J. Phys. G* **32**, 427 (2006).
- [12] L. Adamczyk et al. (STAR Collaboration), *Phys. Rev. C* **88**, 014902 (2013).
- [13] S. A. Bass, M. Belkacem, M. Bleicher, M. Brandstetter, L. Bravina, C. Ernst, L. Gerland, M. Hofmann, S. Hofmann, J. Konopka, G. Mao, L. Neise, S. Soff, C. Spieles, H. Weber, L. A. Winkelmann, H. Stocker, W. Greiner, Ch. Hartnack, J. Aichelin and N. Amelin, *Prog. Part. Nucl. Phys.* **41**, 225-370 (1998).
- [14] M. Bleicher, E. Zabrodin, C. Spieles, S.A. Bass, C. Ernst, S. Soff, L. Bravina, M. Belkacem, H. Weber, H. Stocker, W. Greiner, *J. Phys. G: Nucl. Part. Phys.* **25**, 1859-1896 (1999).
- [15] R. Brun, F. Bruyant, M. Maire, A.C. McPherson, P. Zanmarini, *CERN-DD-EE-84-1* (1987).
- [16] R. Fruehwirth, *Nucl. Instr. and Meth.* **262**, 444 (1987).
- [17] S.P. Merts, S.V. Razin, O.V. Rogachevsky, *Matem. Mod.* **12**, 102 (2012).
- [18] S. Voloshin and Y. Zhang, preprint arXiv:hep-ph/9407282v1 (1994), *Z. Phys. C* **70**, 665 (1996).
- [19] A. M. Poskanzer and S. Voloshin, preprint arXiv:9805001v2 [nucl-ex] (1998), *Phys. Rev. C* no.CS6346 (1998).
- [20] H. Masui and A. Schmah, preprint arXiv:1212.3650v1 [nucl-ex] (2012).
- [21] C. Pinkenburg et al., *Phys. Rev. Lett.* **83**, 1295 (1999).
- [22] P. Braun-Munzinger, J. Stachel *Nucl. Phys.* **638**, 3c (1998).
- [23] H. Appelshäuser et al., *Nucl. Phys.* **698**, 253c (2002).
- [24] R. Luchsinger and Ch. Grab, *Comp. Phys. Comm.* **76**, 263 (1993).

РАЗРАБОТКА НА МЕТОДИ ЗА АНАЛИЗ НА АНИЗОТРОПИЧЕН ПОТОК  
НА ЧАСТИЦИ КЪМ ЕКСПЕРИМЕНТА MPD/NICA

Н. Гераксиев (от името на MPD колектива)

ВБЛФВЕ, Обединен институт за ядрени изследвания, Дубна, Русия

(Резюме)

Измерването на азимуталните анизотропии в разпределението на напречния импулс на частиците може да разкрие информация за ранните етапи в релятивистките сблъсъци на тежки йони. Степента на трансфер от пространствена към импулсна анизотропия зависи от плътността на средата по време на еволюцията на системата след сблъсъка и от сеченията на взаимодействащите частици.

Основна част от работата представя подбор на събитията по централност и методите за реконструкция на плоскостта на сблъсък чрез трекове от времепроекционната камера (TPC) или енергията отложена в калориметъра при нулев градус (ZDC) при експеримента MPD@NICA.

От съществена важност е изследването на страни бариони, поради малкото им сечение на взаимодействие, а като такива специално внимание е отделено на ламбда хипероните.

Представени са резултати от реконструирани събития, генерирани от модела UrQMD 3.3, чрез софтуера на експеримента MPDroot. Получените данни са сравнени с актуални експерименти.